Energy & Environmental Science

COMMUNICATION

View Article Online
View Journal

Cite this: DOI: 10.1039/c5ee01838b

Received 15th June 2015,
Accepted 19th June 2015

DOI: 10.1039/c5ee01838b

www.rsc.org/ees

Diluting concentrated solution: a general, simple and effective approach to enhance efficiency of polymer solar cells†

Pei Cheng,[ad] Cenqi Yan,[b] Yongfang Li,[a] Wei Ma*[c] and Xiaowei Zhan*[b]

Diluting concentrated solution (DCS) is a new, simple, general and effective approach to improve power conversion efficiencies (PCEs) of polymer solar cells (PSCs). PCEs of binary blend PSCs, ternary blend PSCs and all-polymer solar cells fabricated using this method are enhanced by a factor as high as 37% relative to those using the general process.

Polymer solar cells (PSCs) have attracted considerable attention in recent years because of some advantages, such as low cost, light weight, flexibility, simple preparation, semi-transparency and large-area fabrication.[1–9] To date, bulk heterojunction (BHJ) PSCs based on interpenetrating networks of semiconducting polymers and fullerene derivatives have shown power conversion efficiencies (PCEs) >10%[10] for single junction and 11%[11] for tandem structure.

Control of the active layer morphology is as important as synthesis of donor and acceptor materials[12–17] and interfacial engineering,[18–20] and becomes one of the research focuses of PSCs.[21–24] In particular, controlling the dynamics of solvent evaporation during spin-coating (by use of solvent additives[25–30] or mixed solvents[31–33]) and post-treatments after spin-coating (by use of thermal annealing,[34–36] solvent annealing[37–39] or solvent treatments[40–43]) was widely investigated.

However, the aggregate state of active materials in prepared solution is also very important for active layer morphology but was rarely investigated.[44–49] According to the theory of Flory and de Gennes,[50,51] there are three types of polymer solutions in terms of polymer concentration: (1) dilute solution, in which the polymer concentration is lower than the contact concentration (c^*), and the polymers don't contact or entangle; (2) semidilute solution, in which the polymer concentration is between c^* and the entanglement concentration (c_e), and the polymers contact with each other but no entanglement occurs; (3) concentrated solution, in which the polymer concentration is higher than c_e, and the polymers contact and entangle with each other. The polymer aggregate states in these three types of polymer solutions are different and influence the performance of PSCs. For some representative high-efficiency polymer/fullerene systems (*e.g.* PTB7/$PC_{71}BM$,[52] PBDTTT-C-T/$PC_{71}BM$[53]), the concentrations of polymer donors are generally 10 mg ml^{-1}. Although the structures of polymer materials widely used in

Broader context

Polymer solar cells (PSCs) have attracted considerable attention in recent years because of some advantages, such as low cost, light weight, flexibility, simple preparation, semi-transparency and large-area fabrication. Control of the active layer morphology is very important. In particular, controlling the dynamics of solvent evaporation during spin-coating and post-treatment after spin-coating were widely investigated. However, the aggregate state of active materials in prepared solution is also very important for active layer morphology but was rarely investigated. In this work, we report a new, simple, universal and effective approach to enhance the power conversion efficiencies (PCEs) of PSCs through controlling the polymer aggregate state in solution. In order to allow polymers to contact and entangle at high concentrations and to avoid changing the dynamics of solvent evaporation, we prepare a donor : acceptor solution with a very high polymer concentration of 70 mg ml^{-1}, and then dilute it to a low polymer concentration of 10 mg ml^{-1} for spin-coating. The polymer aggregate state in solution may be maintained during dilution, since the diffusion of solvent molecules into polymers is much quicker than the diffusion of polymers into solvent molecules. High original polymer concentration leads to reduced phase separation and the formation of polymer networks in blended films, increased hole mobility and efficient vertical phase separation. PCEs of binary blend PSCs, ternary blend PSCs and all-polymer solar cells fabricated using this method are enhanced by a factor as high as 37% relative to those using an original polymer concentration of 10 mg ml^{-1}.

[a] *Beijing National Laboratory for Molecular Sciences and CAS Key Laboratory of Organic Solids, Institute of Chemistry, Chinese Academy of Sciences, Beijing 100190, China*
[b] *Department of Materials Science and Engineering, College of Engineering, Key Laboratory of Polymer Chemistry and Physics of Ministry of Education, Peking University, Beijing 100871, China. E-mail: xwzhan@pku.edu.cn*
[c] *State Key Laboratory for Mechanical Behavior of Materials, Xi'an Jiaotong University, Xi'an 710049, China*
[d] *University of Chinese Academy of Sciences, Beijing 100049, China*

† Electronic supplementary information (ESI) available: Molecular structures, photovoltaic properties with different processing time and calculation of the surface compositions. See DOI: 10.1039/c5ee01838b

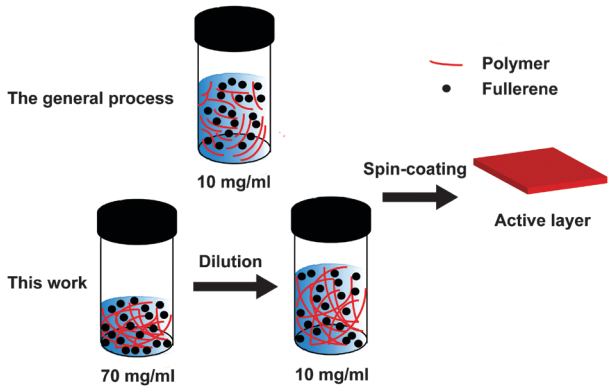

Fig. 1 Schematic diagram of different fabrication processes of devices in this work and the literature.

PSCs are too complicated to obtain c^* and c_e, the general relationship of polymer concentrations and polymer aggregate states can still be used. Polymers with higher concentration have more opportunity to contact and entangle, while polymers with lower concentration have less opportunity to contact and entangle. To control the polymer aggregate states, simply changing polymer concentration needs a changing speed of spin-coating to obtain a similar film thickness, but a change in speed will lead to a change in the dynamics of solvent evaporation, especially for systems with solvent additives.

In this work, in order to allow polymers to contact and entangle at high concentration and to avoid changing the dynamics of solvent evaporation, we explored a new method: diluting concentrated solution (DCS). We prepared a donor : acceptor solution with a very high polymer concentration of 70 mg ml^{-1}, and then diluted it to a low polymer concentration of 10 mg ml^{-1} for spin-coating (Fig. 1). The polymer aggregate state in solution may be maintained during dilution since the diffusion of solvent molecules into polymers is much quicker than the diffusion of polymers into solvent molecules.[50] PTB7 : $PC_{71}BM$ and PBDTTT-C-T : $PC_{71}BM$-based binary blend PSCs, PTB7 : ICBA : $PC_{71}BM$-based ternary blend PSCs and PBDTTT-C-T : PPDIDTT-based all-polymer solar cells fabricated using this method achieved PCEs as high as 7.85%, 7.82%, 8.88% and 4.63%, respectively, which were enhanced by a factor of 6–37% relative to those using an original polymer concentration of 10 mg ml^{-1}. The PCE of 8.88% is the highest reported for ternary blend PSCs based on organic third components,[54–59] while the PCE of 4.63% is among the highest reported for perylene diimide (PDI) polymer acceptor-based all-polymer solar cells.[60–63] This is a new, simple, universal and effective approach to enhance the PCEs of PSCs through controlling the polymer aggregate state in solution.

We used PTB7[52] and PBDTTT-C-T[53] as the donor materials and $PC_{71}BM$, $PC_{71}BM$/ICBA[64] and PPDIDTT[60] as the acceptor materials to fabricate polymer/fullerene and all-polymer solar cells (structures of these molecules are shown in Fig. S1, ESI†). Fig. 2 shows the J–V curves and external quantum efficiency (EQE) spectra of devices based on PTB7 : ICBA : $PC_{71}BM$ blends with different original polymer concentrations under AM 1.5G illumination at an intensity of 100 mW cm^{-2}. Table 1 summarizes the average and best device characteristics of different D/A pairs (PTB7 : $PC_{71}BM$, PTB7 : ICBA : $PC_{71}BM$, PBDTTT-C-T : $PC_{71}BM$, PBDTTT-C-T : PPDIDTT) with different original polymer concentrations. For polymer/fullerene solar cells, the original polymer concentrations of polymers influence the short circuit current density (J_{SC}) and fill factor (FF) but slightly affect the open circuit voltage (V_{OC}). With increasing the original polymer concentrations of polymers from 10 mg ml^{-1} to 70 mg ml^{-1}, the average J_{SC}, FF and PCE increase. The polymer/fullerene solar cells exhibit the best performance when the original polymer concentrations of polymers are 70 mg ml^{-1}; the average PCEs increase from 7.23% to 7.67%, 8.13% to 8.73% and 7.18% to 7.69% for PTB7/$PC_{71}BM$, PTB7/ICBA/$PC_{71}BM$ and PBDTTT-C-T/$PC_{71}BM$, respectively. For all-polymer solar cells, the trend is similar; the J_{SC}, FF and PCE increase with increasing original polymer concentration. Relative to what we reported before (20 mg ml^{-1}),[61] the devices with higher original polymer concentration (80 mg ml^{-1}) exhibit enhanced performance: the average J_{SC}, FF and PCE increase from 8.55 mA cm^{-2}, 51.5% and 3.31% to 9.77 mA cm^{-2}, 60.9% and 4.55%, respectively.

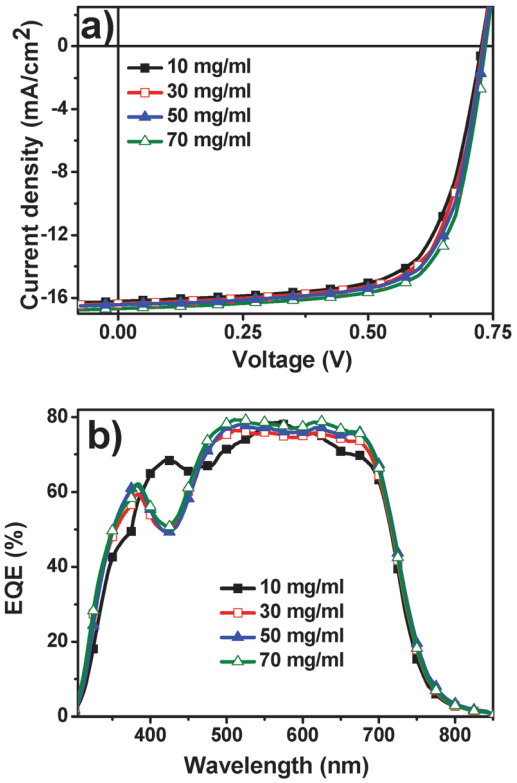

Fig. 2 (a) J–V curves and (b) EQE spectra of devices based on PTB7 : ICBA : $PC_{71}BM$ blends with different original polymer concentrations under the illumination of an AM 1.5G solar simulator, 100 mW cm^{-2}.

As shown in Fig. 2b, the trend of EQE is similar to J_{SC}. The EQE in 450–750 nm range is mainly attributed to PTB7, while that below 450 nm is mainly contributed by $PC_{71}BM$. The EQE related to PTB7 is obviously enhanced by use of higher original polymer concentration. To evaluate the accuracy of the photovoltaic results, the J_{SC} values are calculated from integration of

Table 1 Average and best device characteristics of different D/A pairs with different original polymer concentrations

Active layer	Ratio	Polymer concentration (mg ml^{-1})	V_{OC} (V)	J_{SC} (mA cm^{-2})	Calculated J_{SC} (mA cm^{-2})	FF (%)	PCE (%)	
							Average	Best
PTB7 : $PC_{71}BM$	1 : 1.5	10	0.701	14.99	14.46	68.8	7.23	7.35
PTB7 : $PC_{71}BM$	1 : 1.5	30	0.702	15.27	14.88	69.2	7.42	7.48
PTB7 : $PC_{71}BM$	1 : 1.5	50	0.701	15.28	15.03	70.1	7.51	7.60
PTB7 : $PC_{71}BM$	1 : 1.5	70	0.703	15.45	15.38	70.6	7.67	7.85
PTB7 : ICBA : $PC_{71}BM$	1 : 0.225 : 1.275	10	0.728	16.26	16.02	68.7	8.13	8.24
PTB7 : ICBA : $PC_{71}BM$	1 : 0.225 : 1.275	30	0.731	16.38	16.07	69.8	8.36	8.45
PTB7 : ICBA : $PC_{71}BM$	1 : 0.225 : 1.275	50	0.732	16.44	16.38	70.7	8.51	8.60
PTB7 : ICBA : $PC_{71}BM$	1 : 0.225 : 1.275	70	0.735	16.68	16.55	71.2	8.73	8.88
PBDTTT-C-T : $PC_{71}BM$	1 : 1.5	10	0.765	15.26	15.08	61.5	7.18	7.30
PBDTTT-C-T : $PC_{71}BM$	1 : 1.5	30	0.768	15.36	15.13	62.3	7.35	7.41
PBDTTT-C-T : $PC_{71}BM$	1 : 1.5	50	0.768	15.38	15.11	63.0	7.44	7.58
PBDTTT-C-T : $PC_{71}BM$	1 : 1.5	70	0.771	15.61	15.40	63.9	7.69	7.82
PBDTTT-C-T : PPDIDTT	1 : 1	20	0.752	8.55	8.58	51.5	3.31	3.45
PBDTTT-C-T : PPDIDTT	1 : 1	40	0.757	8.74	8.63	55.8	3.69	3.82
PBDTTT-C-T : PPDIDTT	1 : 1	60	0.760	9.32	8.99	58.7	4.16	4.30
PBDTTT-C-T : PPDIDTT	1 : 1	80	0.765	9.77	9.72	60.9	4.55	4.63

the EQE spectra with the AM 1.5G reference spectrum. The calculated J_{SC} is similar to J–V measurement (the average error is 1.4%, Table 1).

Fig. 3 shows the atomic force microscopy (AFM) height images and phase images of PTB7 : ICBA : $PC_{71}BM$ blends with different original polymer concentrations spin-coated on indium tin oxide (ITO)/poly(3,4-ethylenedioxythiophene) : poly(styrene sulfonate) (PEDOT : PSS) substrates. The blend films with different original polymer concentrations exhibit a typical cluster structure with a lot of aggregated domains and a root-mean-square (RMS) roughness of 1.50 nm (10 mg ml^{-1}), 1.22 nm (30 mg ml^{-1}), 0.917 nm (50 mg ml^{-1}) and 0.706 nm (70 mg ml^{-1}), respectively. The more uniform and smooth films with better contact with calcium (Ca) cathode can reduce charge recombination. As shown in phase images, the higher original polymer concentration induces smaller scale phase separation. The smaller aggregated domains lead to a larger donor/acceptor interfacial area. Moreover, given the fact that the typical exciton diffusion length in the disordered blend layer is about 10 nm, the smaller scale phase separation in the blend film with higher original polymer concentration is favorable for efficient exciton dissociation, leading to higher J_{SC}, FF and PCE compared to that with a lower original polymer concentration. Fig. 4 shows the transmission electron microscopy (TEM) images and the energy filter transmission electron microscopy (EF-TEM)[65] images of PTB7 : ICBA : $PC_{71}BM$ blends with different original polymer concentrations spin-coated on ITO/PEDOT : PSS substrates. The TEM and EF-TEM images show a similar trend of morphology change with change in polymer concentration. These images show the relationship between different original polymer concentrations and polymer networks. The polymer networks (the light part in EF-TEM) become more obvious and continuous with increasing original polymer concentrations. At high original polymer concentrations, the polymer chains tend to be easily contacted and entangled, and the diffusion of polymers is suppressed, leading to the formation of

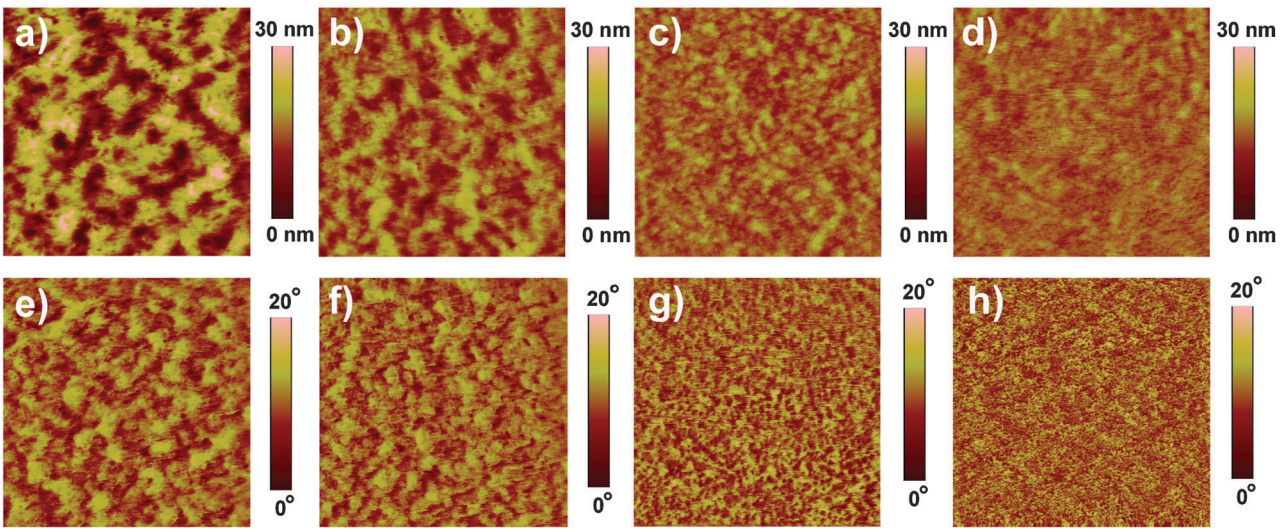

Fig. 3 AFM height images (a–d) and phase images (e–h) of PTB7 : ICBA : $PC_{71}BM$ blends with different original polymer concentrations spin-coated on ITO/PEDOT : PSS substrates: (a, e) 10 mg ml^{-1}; (b, f) 30 mg ml^{-1}; (c, g) 50 mg ml^{-1}; (d, h) 70 mg ml^{-1}. The scan sizes of all AFM height images and phase images are 3 μm × 3 μm and 1.5 μm × 1.5 μm, respectively.

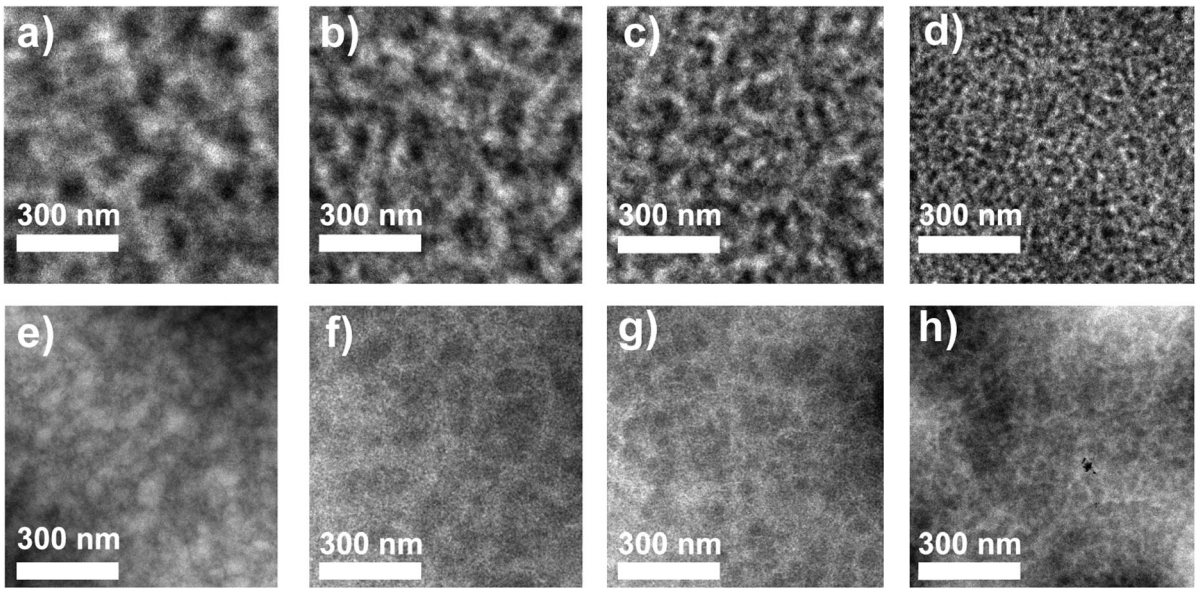

Fig. 4 TEM (a–d) and EF-TEM images (e–h) of PTB7 : ICBA : $PC_{71}BM$ blends with different original polymer concentrations spin-coated on ITO/PEDOT : PSS substrates: (a, e) 10 mg ml^{-1}; (b, f) 30 mg ml^{-1}; (c, g) 50 mg ml^{-1}; (d, h) 70 mg ml^{-1}.

dense polymer networks and small scale phase separation in the blended film.

Grazing-incidence wide-angle X-ray scattering (GIWAXS) was employed to investigate the molecular packing and aggregation of films with different original polymer concentrations. Fig. 5 shows two-dimensional (2D) patterns, and the corresponding out-of-plane and in-plane profiles of films with different original polymer concentrations. PTB7 pure films show very high π–π ordering in the out-of-plane direction, indicating a face-on orientation relative to the substrate. The polymers become more ordered with increasing original polymer concentrations due to the enhanced (300). At high original polymer concentrations, the polymer chains tend to be easily contacted and entangled, which can induce more ordered molecular packing. For the PTB7 : ICBA : $PC_{71}BM$ blended films, the peaks at q = 0.65, 1.3 and 1.95 $Å^{-1}$ indicate fullerene aggregation. These peaks become weaker with increasing original polymer concentration, suggesting that the aggregation of fullerenes is reduced with increasing original polymer concentration, which is consistent with TEM and EF-TEM images.

The hole mobility and electron mobility of PTB7 : ICBA : $PC_{71}BM$ blend films were measured by the space charge limited current (SCLC)[66] method (Fig. 6) and listed in Table 2. Hole-only and electron-only diodes were fabricated using the architectures: ITO/PEDOT : PSS/PTB7 : ICBA : $PC_{71}BM$/gold (Au) for holes and aluminium (Al)/PTB7 : ICBA : $PC_{71}BM$/Al for electrons. The blend films with different original polymer concentrations exhibit a hole mobility ranging from 4.09×10^{-3} to 9.10×10^{-3} $cm^2\ V^{-1}\ s^{-1}$ and an electron mobility ranging from 2.32×10^{-4} to 2.88×10^{-4} $cm^2\ V^{-1}\ s^{-1}$. The hole mobility increases with increasing the original polymer concentrations, while the electron mobility is slightly changed. At high original polymer concentrations, close contact and entanglement the polymer chains lead to strong interchain interactions and dense polymer networks, which is attributed to the improvement in hole mobility.

In order to investigate the vertical phase separation of blend films with different original polymer concentrations, we use X-ray photoelectron spectroscopy (XPS) to measure the ratio of atoms and estimate donor/acceptor ratios at the top surface. Since ICBA does not contain heteroatoms and it is impossible to estimate donor/acceptor ratios in PTB7 : ICBA : $PC_{71}BM$, we choose PTB7 : $PC_{71}BM$ to study the vertical phase separation affected by original polymer concentration. The XPS survey scans of PTB7 : $PC_{71}BM$ blend films with different original polymer concentrations are shown in Fig. 7c. Since PTB7 contains sulfur, and both PTB7 and $PC_{71}BM$ contain oxygen, we attribute the sulfur 2p (S 2p) spectral line (~160 eV) to PTB7 and oxygen 1s (O 1s) spectral line (~530 eV) to PTB7 and $PC_{71}BM$. One PTB7 repeat unit contains four S atoms and four O atoms, while one $PC_{71}BM$ molecule contains two O atoms. Top surface compositions of PTB7 : $PC_{71}BM$ with different original polymer concentrations can be calculated from the O/S ratio (ESI†), and are listed in Table 3. The top surface ratios of PTB7 : $PC_{71}BM$ with low original polymer concentration (10 mg ml^{-1}) and high original polymer concentration (70 mg ml^{-1}) are 32.7% : 67.3% and 24.1% : 75.9%, respectively. In polymer/fullerene blended films, the donor polymer tends to aggregate on the top surface due to its relatively low surface energy (proved by the relatively large contact angle) compared with the fullerene acceptor (Fig. 7a and b). At higher original polymer concentration, polymer chain entanglement and the dense polymer network suppresses the migration of polymers to the top surface. As a result, higher original polymer concentration leads to lower polymer donor content and higher fullerene acceptor content at the top surface, which is beneficial to electron collection at the cathode.

In summary, we report a new, simple, general and effective method to improve the efficiency of polymer solar cells. We prepare the donor : acceptor solution with a very high polymer concentration of 70 mg ml^{-1}, which allows the polymers to contact

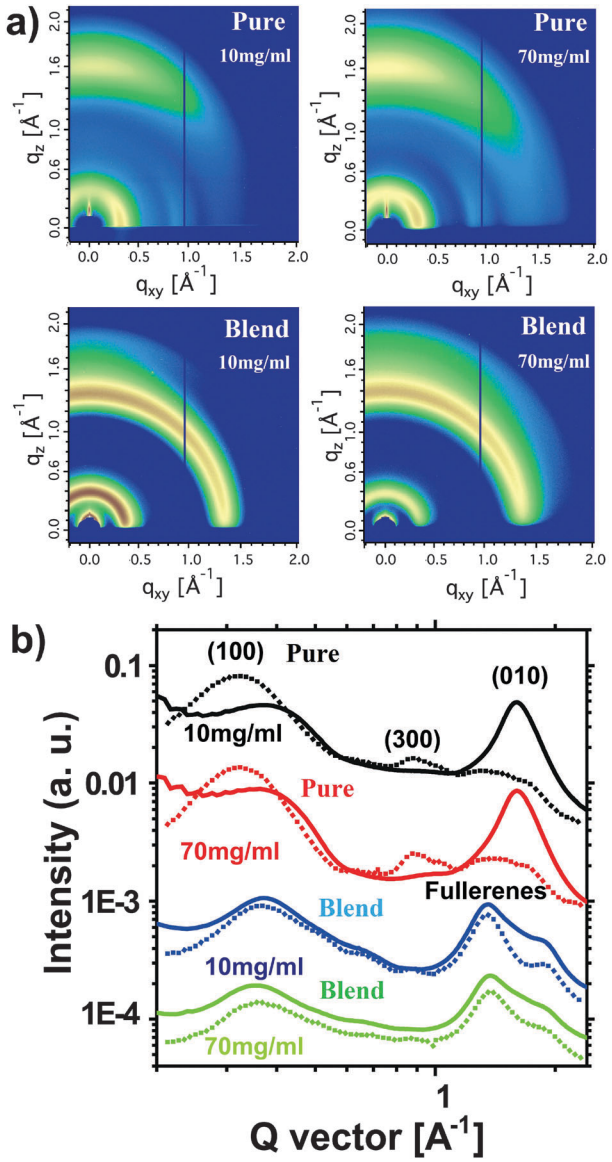

Fig. 5 2D patterns (a) out-of-plane and in-plane (b) GIWAXS data of films with different original polymer concentrations: PTB7 10 mg ml^{-1}, PTB7 70 mg ml^{-1}, PTB7 : ICBA : $PC_{71}BM$ 10 mg ml^{-1}, PTB7 : ICBA : $PC_{71}BM$ 70 mg ml^{-1}. The dashed lines are in-plane data.

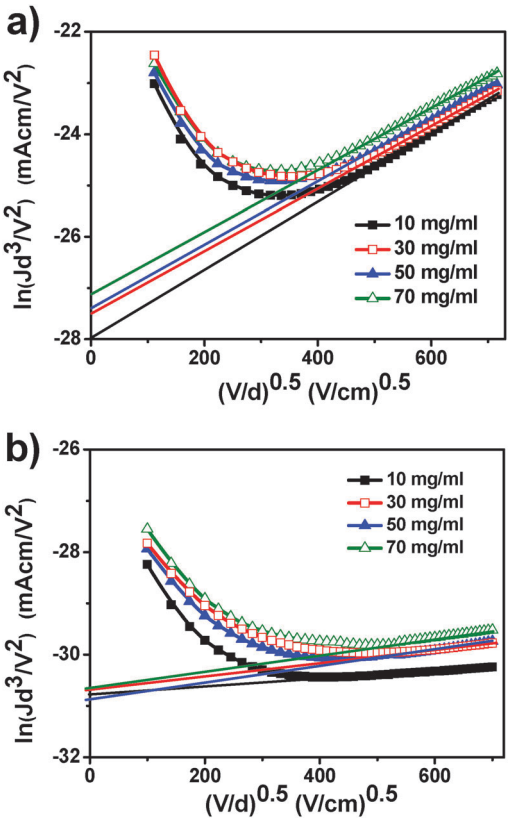

Fig. 6 *J–V* characteristics in the dark for (a) hole-only and (b) electron-only devices based on PTB7 : ICBA : $PC_{71}BM$ blends with different original polymer concentrations.

Table 2 Hole mobilities and electron mobilities of PTB7 : ICBA : $PC_{71}BM$ blends with different original polymer concentrations

Active layer	Polymer concentration (mg ml^{-1})	μ_h (cm^2 V^{-1} s^{-1})	μ_e (cm^2 V^{-1} s^{-1})
PTB7 : ICBA : $PC_{71}BM$	10	4.09×10^{-3}	2.61×10^{-4}
PTB7 : ICBA : $PC_{71}BM$	30	6.74×10^{-3}	2.80×10^{-4}
PTB7 : ICBA : $PC_{71}BM$	50	7.45×10^{-3}	2.32×10^{-4}
PTB7 : ICBA : $PC_{71}BM$	70	9.10×10^{-3}	2.88×10^{-4}

and entangle, then dilute it to a regular polymer concentration (10 mg ml^{-1}) for spin-coating. The higher original polymer concentration leads to smaller phase separation and the formation of polymer networks in blended films, increased hole mobility and efficient vertical phase separation. After optimization of the original polymer concentration, the efficiencies of binary blend polymer solar cells, ternary blend polymer solar cells and all-polymer solar cells are enhanced by a factor of 6–37%.

Experimental section

Unless stated otherwise, solvents and chemicals were obtained commercially and used without further purification. PTB7,[52] PBDTTT-C-T[53] and $PC_{71}BM$ (purity >99.0%) were purchased from Solarmer Materials Inc. and American Dye Inc. PPDIDTT,[60] ICBA[64] and PDI-2DTT[67] (non-volatile additive) were synthesized according to our previous reports. 1,8-Diiodooctane (DIO) and *o*-dichlorobenzene (DCB) were obtained from J&K Chemical Inc. Polymer/fullerene and all-polymer solar cells were fabricated with the structure ITO/PEDOT : PSS/active layer/Ca/Al. The ITO glass (sheet resistance = 10 Ω □$^{-1}$) was pre-cleaned in an ultrasonic bath of acetone and isopropanol, and treated in an ultraviolet-ozone chamber (Jelight Company, USA) for 20 min. A thin layer (35 nm) of PEDOT : PSS (Baytron PVP AI 4083, Germany) was spin-coated onto the ITO glass and baked at 150 °C for 20 min. A mixture of polymer : $PC_{71}BM$ was dissolved in DCB solvent (1 : 1.5, 25 or 75 or 125 or 175 mg ml^{-1} in total) with stirring overnight, then diluted to 25 mg ml^{-1} in total without stirring and kept for over 3 h. Afterwards, this polymer/fullerene

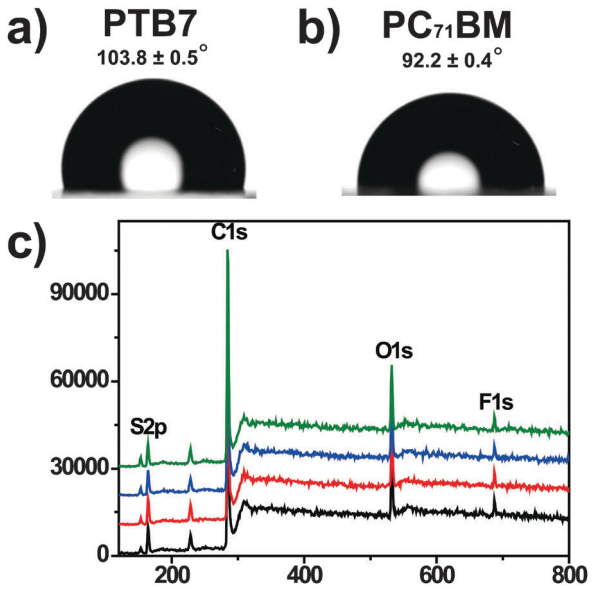

Fig. 7 The static contact angles of (a) PTB7 film and (b) $PC_{71}BM$ film, (c) XPS survey scans of PTB7 : $PC_{71}BM$ blended films with different original polymer concentrations (from bottom to top is 10, 30, 50 and 70 mg ml^{-1}, respectively).

Table 3 Top surface compositions of PTB7 : $PC_{71}BM$ blends with different original polymer concentrations

			PTB7 : $PC_{71}BM$	
Active layer	Polymer concentration	Atom ratio of O/S	Molar ratio (%)	Weight ratio (%)
PTB7 : $PC_{71}BM$	10	1.722	40.9 : 59.1	32.7 : 67.3
PTB7 : $PC_{71}BM$	30	1.836	37.4 : 62.6	29.6 : 70.4
PTB7 : $PC_{71}BM$	50	1.922	35.2 : 64.8	27.6 : 72.4
PTB7 : $PC_{71}BM$	70	2.107	31.1 : 68.9	24.1 : 75.9

solution with 3% DIO was spin-coated on the PEDOT : PSS layer to form a photosensitive layer. Similarly, a mixture of PBDTTT-C-T : PPDIDTT was dissolved in DCB solvent (1 : 1, 20 or 40 or 60 or 80 mg ml^{-1} in total) with stirring overnight, then diluted to 20 mg ml^{-1} in total without stirring and kept for over 3 h. Different processing times slightly affected the device performance (Table S1, ESI†). Afterwards, this all-polymer solution with 2% non-volatile additive PDI-2DTT and 6% DIO was spin-coated on the PEDOT : PSS layer to form a photosensitive layer. The thickness of the active layer based on polymer/fullerene and polymer/polymer blended films was 100 and 70 nm, respectively, as measured by Ambios Technology XP-2 profilometer. A Ca (*ca.* 20 nm) and Al layer (*ca.* 80 nm) was then evaporated onto the surface of the photosensitive layer under vacuum (*ca.* 10^{-5} Pa) to form the negative electrode. The active area of the device was 4 mm^2.

The *J–V* curve was measured using a computer-controlled B2912A Precision Source/Measure Unit (Agilent Technologies). An XES-70S1 (SAN-EI Electric Co., Ltd) solar simulator (AAA grade, 70 × 70 mm^2 photobeam size) coupled with AM 1.5G solar spectrum filters was used as the light source, and the optical power at the sample was 100 mW cm^{-2}. A 2 × 2 cm^2 monocrystalline silicon reference cell (SRC-1000-TC-QZ) was purchased from VLSI Standards Inc. The EQE spectrum was measured using a Solar Cell Spectral Response Measurement System QE-R3011 (Enlitech Co., Ltd). The light intensity at each wavelength was calibrated using a standard single crystal Si photovoltaic cell. The nanoscale morphology of blended films was observed by an atomic force microscope (AFM) (NanoMan VS, Veeco, USA) in contact mode. The transmission electron microscopy (TEM) characterization was carried out on JEM-1011. The energy filter transmission electron microscopy (EF-TEM) characterization was carried out on a Tecnai G2 F20 U-TWIN. The samples for the TEM and EF-TEM measurements were prepared as follows: the active-layer films were spin-cast onto ITO/PEDOT : PSS substrates, and the substrates with the active layers were submerged in deionized water to make the active layers float on the air–water interface. Then, the floated films were picked up on unsupported 200 mesh copper grids for the TEM and EF-TEM measurements. GIWAXS measurements were performed at beamline 7.3.3 at the Advanced Light Source, Berkeley, USA. GIWAXS samples were prepared on Si substrates. The incident angle was 0.14°, which maximized the scattering intensity from the samples. The scattered X-rays were detected using a Dectris Pilatus 2M photon counting detector. Hole-only or electron-only diodes were fabricated using the architectures ITO/PEDOT : PSS/active layer/Au for holes and Al/active layer/Al for electrons. Mobilities were extracted by fitting the current density–voltage curves using the Mott–Gurney relationship (space charge limited current). Static contact angles were measured on a dataphysics OCA20 contact-angle system at ambient temperature (the test liquid is water). X-ray photoelectron spectroscopy (XPS) was performed on the Thermo Scientific ESCALab 250Xi using 200 W monochromated Al Kα radiation. The 500 μm X-ray spot was used for XPS analysis. The base pressure in the analysis chamber was about 3 × 10^{-10} mbar. Typically, the hydrocarbon C 1s line at 284.8 eV from adventitious carbon was used as an energy reference.

Acknowledgements

We thank the NSFC (91433114, 51261130582, 21025418), the 973 Program (2011CB808401), the Chinese Academy of Sciences for financial support.

Notes and references

1 C. J. Brabec, M. Heeney, I. McCulloch and J. Nelson, *Chem. Soc. Rev.*, 2011, **40**, 1185.
2 Y.-J. Cheng, S.-H. Yang and C.-S. Hsu, *Chem. Rev.*, 2009, **109**, 5868.
3 Y. F. Li, *Acc. Chem. Res.*, 2012, **45**, 723.
4 J. Peet, A. J. Heeger and G. C. Bazan, *Acc. Chem. Res.*, 2009, **42**, 1700.
5 G. Li, R. Zhu and Y. Yang, *Nat. Photonics*, 2012, **6**, 153.
6 Y. Lin, Y. Li and X. Zhan, *Chem. Soc. Rev.*, 2012, **41**, 4245.
7 X. Zhao and X. Zhan, *Chem. Soc. Rev.*, 2011, **40**, 3728.

8 M. Hösel, D. Angmo, R. R. Søndergaard, G. A. dos Reis Benatto, J. E. Carlé, M. Jørgensen and F. C. Krebs, *Adv. Sci.*, 2014, **1**, 1400002.
9 S. B. Darling and F. You, *RSC Adv.*, 2013, **3**, 17633.
10 Y. Liu, J. Zhao, Z. Li, C. Mu, W. Ma, H. Hu, K. Jiang, H. Lin, H. Ade and H. Yan, *Nat. Commun.*, 2014, **5**, 5293.
11 A. R. B. M. Yusoff, D. Kim, H. P. Kim, F. K. Shneider, W. J. da Silva and J. Jang, *Energy Environ. Sci.*, 2015, **8**, 303.
12 L. Ye, S. Zhang, L. Huo, M. Zhang and J. Hou, *Acc. Chem. Res.*, 2014, **47**, 1595.
13 J.-S. Wu, S.-W. Cheng, Y.-J. Cheng and C.-S. Hsu, *Chem. Soc. Rev.*, 2015, **44**, 1113.
14 Y. Chen, X. Wan and G. Long, *Acc. Chem. Res.*, 2013, **46**, 2645.
15 X. Guo, A. Facchetti and T. J. Marks, *Chem. Rev.*, 2014, **114**, 8943.
16 X. Zhan, A. Facchetti, S. Barlow, T. J. Marks, M. A. Ratner, M. R. Wasielewski and S. R. Marder, *Adv. Mater.*, 2011, **23**, 268.
17 J. E. Anthony, A. Facchetti, M. Heeney, S. R. Marder and X. Zhan, *Adv. Mater.*, 2010, **22**, 3876.
18 C. Duan, K. Zhang, C. Zhong, F. Huang and Y. Cao, *Chem. Soc. Rev.*, 2013, **42**, 9071.
19 H.-L. Yip and A. K. Y. Jen, *Energy Environ. Sci.*, 2012, **5**, 5994.
20 F. Wang, Z. A. Tan and Y. Li, *Energy Environ. Sci.*, 2015, **8**, 1059.
21 M. T. Dang, L. Hirsch, G. Wantz and J. D. Wuest, *Chem. Rev.*, 2013, **113**, 3734.
22 Y. Huang, E. J. Kramer, A. J. Heeger and G. C. Bazan, *Chem. Rev.*, 2014, **114**, 7006.
23 F. Liu, Y. Gu, X. Shen, S. Ferdous, H.-W. Wang and T. P. Russell, *Prog. Polym. Sci.*, 2013, **38**, 1990.
24 W. Chen, M. P. Nikiforov and S. B. Darling, *Energy Environ. Sci.*, 2012, **5**, 8045.
25 Y. Sun, G. C. Welch, W. L. Leong, C. J. Takacs, G. C. Bazan and A. J. Heeger, *Nat. Mater.*, 2012, **11**, 44.
26 E. Wang, Z. Ma, Z. Zhang, K. Vandewal, P. Henriksson, O. Inganäs, F. Zhang and M. R. Andersson, *J. Am. Chem. Soc.*, 2011, **133**, 14244.
27 W. Li, W. S. C. Roelofs, M. Turbiez, M. M. Wienk and R. A. J. Janssen, *Adv. Mater.*, 2014, **26**, 3304.
28 Y. Kim, H. R. Yeom, J. Y. Kim and C. Yang, *Energy Environ. Sci.*, 2013, **6**, 1909.
29 J. A. Bartelt, J. D. Douglas, W. R. Mateker, A. E. Labban, C. J. Tassone, M. F. Toney, J. M. J. Fréchet, P. M. Beaujuge and M. D. McGehee, *Adv. Energy Mater.*, 2014, **4**, 1301733.
30 H.-C. Liao, C.-C. Ho, C.-Y. Chang, M.-H. Jao, S. B. Darling and W.-F. Su, *Mater. Today*, 2013, **16**, 326.
31 A. J. Moule and K. Meerholz, *Adv. Mater.*, 2008, **20**, 240.
32 F. Liu, Y. Gu, C. Wang, W. Zhao, D. Chen, A. L. Briseno and T. P. Russell, *Adv. Mater.*, 2012, **24**, 3947.
33 L. Ye, S. Zhang, W. Ma, B. Fan, X. Guo, Y. Huang, H. Ade and J. Hou, *Adv. Mater.*, 2012, **24**, 6335.
34 G. Zhao, Y. He and Y. Li, *Adv. Mater.*, 2010, **22**, 4355.
35 W. Ma, C. Yang, X. Gong, K. Lee and A. J. Heeger, *Adv. Funct. Mater.*, 2005, **15**, 1617.
36 P. Cheng, J. Hou, Y. Li and X. Zhan, *Adv. Energy Mater.*, 2014, **4**, 1301349.
37 G. Li, V. Shrotriya, J. S. Huang, Y. Yao, T. Moriarty, K. Emery and Y. Yang, *Nat. Mater.*, 2005, **4**, 864.
38 G. D. Wei, S. Y. Wang, K. Sun, M. E. Thompson and S. R. Forrest, *Adv. Energy Mater.*, 2011, **1**, 184.
39 P. Zalar, M. Kuik, N. A. Ran, J. A. Love and T.-Q. Nguyen, *Adv. Energy Mater.*, 2014, **4**, 1400438.
40 Z. Xiao, Y. Yuan, B. Yang, J. VanDerslice, J. Chen, O. Dyck, G. Duscher and J. Huang, *Adv. Mater.*, 2014, **26**, 3068.
41 H. Zhou, Y. Zhang, J. Seifter, S. D. Collins, C. Luo, G. C. Bazan, T.-Q. Nguyen and A. J. Heeger, *Adv. Mater.*, 2013, **25**, 1646.
42 L. Ye, Y. Jing, X. Guo, H. Sun, S. Zhang, M. Zhang, L. Huo and J. Hou, *J. Phys. Chem. C*, 2013, **117**, 14920.
43 J. Kong, I.-W. Hwang and K. Lee, *Adv. Mater.*, 2014, **26**, 6275.
44 K. Zhao, H. U. Khan, R. Li, Y. Su and A. Amassian, *Adv. Funct. Mater.*, 2013, **23**, 6024.
45 M. Chang, J. Lee, P.-H. Chu, D. Choi, B. Park and E. Reichmanis, *ACS Appl. Mater. Interfaces*, 2014, **6**, 21541.
46 Y.-W. Su, C.-M. Liu, J.-M. Jiang, C.-S. Tsao, H.-C. Cha, U. S. Jeng, H.-L. Chen and K.-H. Wei, *J. Phys. Chem. C*, 2015, **119**, 3408.
47 M. Wirix, P. Bomans, M. Hendrix, H. Friedrich, N. Sommerdijk and G. de With, *J. Mater. Chem. A*, 2015, **3**, 5031.
48 S. Cho, B. S. Rolczynski, T. Xu, L. Yu and L. X. Chen, *J. Phys. Chem. B*, 2015, **119**, 7447.
49 Z. Guo, D. Lee, H. Gao and L. Huang, *J. Phys. Chem. B*, 2015, **119**, 7666.
50 P. J. Flory, *Principles of Polymer Chemistry*, Connell University Press, New York, USA, 1971.
51 P. G. de Gennes, *Scaling Concepts in Polymer Physics*, Connell University Press, New York, USA, 1979.
52 Y. Liang, Z. Xu, J. Xia, S.-T. Tsai, Y. Wu, G. Li, C. Ray and L. Yu, *Adv. Mater.*, 2010, **22**, E135.
53 L. J. Huo, S. Q. Zhang, X. Guo, F. Xu, Y. F. Li and J. H. Hou, *Angew. Chem., Int. Ed.*, 2011, **50**, 9697.
54 P. Cheng, Y. Li and X. Zhan, *Energy Environ. Sci.*, 2014, **7**, 2005.
55 L. Lu, T. Xu, W. Chen, E. S. Landry and L. Yu, *Nat. Photonics*, 2014, **8**, 716.
56 Y. Yang, W. Chen, L. Dou, W.-H. Chang, H.-S. Duan, B. Bob, G. Li and Y. Yang, *Nat. Photonics*, 2015, **9**, 190.
57 Y. Zhang, D. Deng, K. Lu, J. Zhang, B. Xia, Y. Zhao, J. Fang and Z. Wei, *Adv. Mater.*, 2015, **27**, 1071.
58 Y. Huang, W. Wen, S. Mukherjee, H. Ade, E. J. Kramer and G. C. Bazan, *Adv. Mater.*, 2014, **26**, 4168.
59 K. Yao, Y.-X. Xu, F. Li, X. Wang and L. Zhou, *Adv. Opt. Mater.*, 2015, **3**, 321.
60 X. Zhan, Z. A. Tan, B. Domercq, Z. An, X. Zhang, S. Barlow, Y. Li, D. Zhu, B. Kippelen and S. R. Marder, *J. Am. Chem. Soc.*, 2007, **129**, 7246.
61 P. Cheng, L. Ye, X. Zhao, J. Hou, Y. Li and X. Zhan, *Energy Environ. Sci.*, 2014, **7**, 1351.
62 Y. Zhou, T. Kurosawa, W. Ma, Y. Guo, L. Fang, K. Vandewal, Y. Diao, C. Wang, Q. Yan, J. Reinspach, J. Mei, A. L. Appleton,

G. I. Koleilat, Y. Gao, S. C. B. Mannsfeld, A. Salleo, H. Ade, D. Zhao and Z. Bao, *Adv. Mater.*, 2014, **26**, 3767.
63 E. J. Zhou, J. Z. Cong, Q. S. Wei, K. Tajima, C. H. Yang and K. Hashimoto, *Angew. Chem., Int. Ed.*, 2011, **50**, 2799.
64 Y. J. He, H. Y. Chen, J. H. Hou and Y. F. Li, *J. Am. Chem. Soc.*, 2010, **132**, 1377.
65 J. Wen, D. J. Miller, W. Chen, T. Xu, L. Yu, S. B. Darling and N. J. Zaluzec, *Microsc. Microanal.*, 2014, **20**, 1507.
66 G. G. Malliaras, J. R. Salem, P. J. Brock and C. Scott, *Phys. Rev. B: Condens. Matter Mater. Phys.*, 1998, **58**, 13411.
67 X. W. Zhan, Z. A. Tan, E. J. Zhou, Y. F. Li, R. Misra, A. Grant, B. Domercq, X. H. Zhang, Z. S. An, X. Zhang, S. Barlow, B. Kippelen and S. R. Marder, *J. Mater. Chem.*, 2009, **19**, 5794.

